Low-Dose 68 Ga-PSMA Prostate PET/MRI Imaging Using Deep Learning Based On MR Priors

Fuquan Deng
Shenzhen Institute of Advanced Technology
Xiaoyuan Li
Nanjing Medical University
Fengjiao Yang
Nanjing Medical University
Hongwei Sun
United Imaging Research Institute of Intelligent Imaging
Jianmin Yuan
United Imaging Healthcare Group
Qiang He
United Imaging Healthcare Group
Weifeng Xu
North China Electric Power University
YongFeng Yang
Shenzhen Institute of Advanced Technology
Dong Liang
Shenzhen Institute of Advanced Technology
Xin Liu
Shenzhen Institute of Advanced Technology
Hairong Zheng
Shenzhen Institute of Advanced Technology
zhanli hu (zl.hu@siat.ac.cn)
Shenzhen Institute of Advanced Technology https://orcid.org/0000-0003-0618-6240

Research Article

Keywords: PET/MRI, prostate, low-dose restoration, deep learning, discrete wavelet transform

Posted Date: October 19th, 2021

DOI: https://doi.org/10.21203/rs.3.rs-972414/v1

Version of Record: A version of this preprint was published at Frontiers in Oncology on January 26th, 2022. See the published version at https://doi.org/10.3389/fonc.2021.818329.

Abstract

Purpose: 68 Ga-prostate-specific membrane antigen (PSMA) PET/MRI has become an effective imaging method for prostate cancer. The purpose of this study was to use deep learning methods to perform low-dose image restoration on PSMA PET/MRI and to evaluate the effect of synthesis on the images and the medical diagnosis of patients at risk of prostate cancer.

Methods: We reviewed the 68 Ga-PSMA PET/MRI data of 41 patients. The low-dose PET images of these patients were restored to full-dose PET images through a deep learning method based on MR priors. The synthesized images were evaluated according to quantitative scores from nuclear medicine doctors and multiple imaging indicators, such as peak-signal noise ratio (PSNR), structural similarity (SSIM), normalization mean square error (NMSE), and relative contrast-to-noise ratio (RCNR).

Results: The scores of the full images synthesized from 25%- and 50%-dose images based on MR priors were 3.84±0.36 and 4.03±0.17, respectively, which were higher than the scores of the target images. Correspondingly, the PSNR, SSIM, NMSE, and RCNR values of the full-dose images synthesized from 25%-dose PET images based on MR priors were 37.86±4.16, 0.916±0.063, 0.015±0.012, and 1.004±0.126, respectively.

Conclusion: According to a combination of quantitative scores from nuclear medicine doctors and evaluations with multiple image indicators, the synthesis of full-dose images based on MR priors using 25%- and 50%-dose PET images did not affect the clinical diagnosis of prostate cancer. Prostate cancer patients can undergo 68 Ga-PSMA prostate PET/MRI scans with radiation doses reduced by up to 75% through the use of deep learning methods to synthesize full-dose images.

Introduction

Prostate cancer is one of the most common cancers worldwide, with approximately 1.41 million new cases reported in 2020, the third most common among 36 cancers [1]. In recent years, studies have demonstrated that 68 Ga-prostate-specific membrane antigen (PSMA) PET/MRI provides accurate staging of primary prostate cancer with a high detection rate [2–6]. In terms of evaluating recurrent prostate cancer, this imaging technique also has a high detection rate, even for patients with extremely low levels of prostate specific antigen (PSA; <0.5 ng/ml). Additionally, it plays an important role in tumor detection, preliminary staging, treatment response assessment, and treatment planning [7, 8].

However, this technique also has some limitations, including scanning time, the cost of the associated radiopharmaceuticals, and the radiation delivered by PET imaging [9]. The economic factors and radiation risks have different kinds of impact on the patients. The purpose of reducing the dose of radiopharmaceuticals is related to the potential risks of ionizing radiation. To reduce the risk of radiation exposure that those involved in the scan may face, especially pediatric patients and volunteers, or when a variety of different tracers are used for follow-up or to monitor treatment response, fewer radiopharmaceuticals should be used to perform PET imaging. The reduction in the number of

radiopharmaceuticals will reduce the quality of the PET images, thereby affecting quantitative analysis and clinical diagnosis.

Researchers have proposed a variety of methods to ensure that the synthesized full-dose PET images have the same image quality as the clinical diagnostic images [10–12]. In particular, deep learning has shown great potential in recovering low-dose PET images. Yan Wang et al used a 3D conditional generative adversarial network (GAN) to synthesize standard-dose images from low-dose head PET images [13]. Wenzhuo Lu et al used a fully optimized 3D U-net to effectively reduce the noise in low-dose PET images from the lungs while minimizing the deviation in the lung nodules [14]. Yang Lei et al proposed using CycleGAN to estimate full-dose prostate PET images from low-dose prostate PET images [15]. Long Zhou et al also used CycleGAN, denoising low-dose fluorodeoxyglucose (FDG) PET images and subsequently performing quantitative analysis on the images [16].

In this study, we retrospectively analyzed the 68 Ga-PSMA PET/MRI data of 41 patients in Nanjing First Hospital. The PET images were reconstructed at acquisition times of 2.5%, 5%, 25%, 50%, and 100% of the standard acquisition time. A discrete-wavelet-transform convolutional neural network (DWTN) was used to restore the low-dose PET images to the original, full-dose PET images with or without the use of MR priors, respectively, to explore the extent to which this method can reduce the required radiotracer dose.

Materials And Methods

PET/MRI data acquisition

In this study, we used clinical images obtained from 68 Ga-PSMA PET/MR examinations performed at Nanjing First Hospital from January 2021 to July 2021. The data were obtained from 41 male patients who might present with signs of future prostate cancer. The mean age of the patients was 67±6 years, and the mean weight was 73±10 kg. Sixty minutes after the patient had been injected with 68 Ga-PSMA (in the range of 111-185×10^6 MBq), scanning data were collected from the PET/MR scanner (United Imaging Healthcare, uPMR 790). The acquisition time of emission images was 600 s, and the PET images were reconstructed at acquisition times of 600, 300, 150, 30, and 15 s.

All PET images were reconstructed using ordered subset expectation maximization (OSEM) and a set series of parameters, for example, 3D iterative time-of-flight (TOF) and point-spread function (PSF) reconstruction, 2 iterations, 20 subsets, matrix 192×192, slice thickness 2.5 mm, and correction methods such as decay correction, attenuation correction, scatter correction, dead time correction, random correction, and detector normalization correction. The images reconstructed at the acquisition times above correspond to 100%-, 50%-, 25%-, 5%-, and 2.5%-dose (low-dose) PET images, respectively. The water sequence decomposed from the T1-weighted MR images was used as the prior images for generating the low-dose PET images.

Since integrated prostate PET/MRI was used for scanning, the PET and MRI scans were coaxial. The PET image matrix size is 192×192, and the MRI image matrix size is 552×387. To ensure that the image resolution was not lower than that of the original image, we used bicubic interpolation to export the two modal images as a 512×512 matrix. Since the image matrix sizes of the two modalities are now the same, the images of the two modalities do not need to be registered. In total, the 41 patients had 4100 sets of images, 5% of which were used as the test set, while the remaining images were used as the training set. To avoid overfitting due to the small size of the data set, we increased the number of images in the training data set by flipping the images down, left and right, quadrupling the size of the training data set. This process helped improve the generalizability of the deep learning models.

Discrete-wavelet-transform convolutional neural network

The DWTN proposed in this study is an improvement of the densely self-guided wavelet network (DSWN) [17], which is suitable for low-dose PET image restoration tasks based on MRI priors. The structure of the DWTN is the same as that of the DSWN. The multilayer self-guided architecture makes better use of multiscale image information; low-resolution feature information from the top layer is gradually fused with higher-resolution feature information to improve the network's ability to extract multiscale feature information from images. Wavelet transform is used instead of ordinary upsampling and downsampling and PixelShuffle and PixelUnshuffle to generate multiscale image information. Before the convolution process, the image is converted into horizontal, vertical, and diagonal detail images and thumbnails through discrete wavelet transform [18]. At the full-resolution layer, the main branch and attention branch provide stability and process the feature images. At each layer, we add densely connected residual blocks to improve the convergence of the network. The top layer of the DWTN extracts large-scale image feature information in the lowest resolution space. The top-level network contains two convolution layers, a leaky ReLU layer, and a densely connected residual (DCR) block [19]. The DCR block consists of three convolutional layers, each of which is followed by a leaky ReLU. Each feature image is connected by dense connections so that our model can use the previous feature information to solve the gradient disappearance problem. The middle two layers are similar to the top layer. For the full-resolution level, we add multiple DCR blocks after merging the multiscale feature information to enhance the feature extraction capability of the DWTN. For the attention branch, we add a tanh activation function after the two DCR blocks. The main branch and the attention branch are processed and added, and then through multiple residual blocks and convolution blocks, the added image feature information is extracted. Finally, through a convolution block without an activation function, the details of the image are preserved. The last convolution layer uses a 1×1 convolution kernel with a step count of 1, and the remaining convolution layers all use a 3×3 convolution kernel with a step count of 1. When initializing the training parameters, the learning rate is set to 0.001, and the remaining parameters are set to their default values.

We update the learning rate every 25 epochs and set the learning rate decay rate to 0.5. The weights of all hidden layers are initialized with Gaussian random numbers. The model was implemented on an NVIDIA GeForce RTX 2080Ti GPU with 11 GB of memory and run under the Microsoft Windows 10 operating system. During training, we used a batch size of 4 for 100 epochs.

Evaluation strategy

Clinical quantitative evaluation. To evaluate the quality of the PET images, we evaluated the original low-dose images, the synthesized full-dose PET images, and the synthesized full-dose PET images based on the MR priors. There were 13 sets of images, including 32 PET images in each group. The PET images were evaluated using a 5-point method by two nuclear medicine physicians from Nanjing First Hospital [20, 21].

Image quantitative analysis. To evaluate the image quality between the synthesized full-dose PET images and the original full-dose PET images, we used the peak-signal noise ratio (PSNR), structural similarity (SSIM), relative contrast-to-noise ratio (RCNR), and normalized mean square error (NMSE) as objective indicators. The PSNR is a quantitative index for evaluating images and noise, and the SSIM is an index for evaluating the similarity of two image features; both indices offer comprehensive evaluations of two images. The NMSE is an indicator of the quantitative analysis of two images at the pixel level. The contrast-to-noise ratio (CNR) is an objective index used to evaluate the quality of medical images; the RCNR is a dimensionless image index based on CNR that is used to compare the contrast of two images.

Results

Compared with the low-dose images, the full-dose images synthesized by the deep learning method demonstrated significantly improved image quality. PET images with a dose of less than 5% showed irregular spots, and their contours, shapes, and contrast were different from those of the target images. In the images synthesized from those with a dose of less than 5%, the spots were eliminated, and the shape features and contrast were relatively consistent with those of the target images. In PET images with a dose greater than 5%, the contours, shapes, and contrast were similar to those the target images, but subtle differences could be observed. In the synthesized PET images, the shapes, contours, and contrast were consistent with those of the target images.

After training the model, we calculated the mean and standard deviation of the RCNR, PSNR, SSIM, NMSE among the original low-dose PET original image, the synthesized full-dose images, the prior-synthesized full-dose images, and the target images of all doses in the test set. Table 1 shows the mean and standard deviation values of the image indicators. To more intuitively visualize the differences in these image indicators, Fig. 2 shows the histograms of the structural similarity and NMSE indicators. The processed low-dose images had significantly better image quality than the original low-dose PET images. The images based on MR prior synthesis showed better image quality at the global-feature and pixel levels.

Table 1
Objective indicators for low-dose PET images, synthesized full-dose PET images, MR prior-synthesized full-dose PET images, and target images.

Image	PSNR	SSIM	NMSE	RCNR
2.5%	25.56 ± 4.99	0.745 ± 0.112	0.065 ± 0.045	0.835 ± 0.267
2.5%PET	32.51 ± 4.89	0.820 ± 0.079	0.029 ± 0.021	1.046 ± 0.213
2.5%PET+MR	33.34 ± 4.47	0.846 ± 0.060	0.026 ± 0.018	1.118 ± 0.218
5%	26.99 ± 5.56	0.756 ± 0.113	0.057 ± 0.037	0.860 ± 0.227
5%PET	33.25 ± 4.57	0.814 ± 0.137	0.026 ± 0.018	1.032 ± 0.216
5%PET+MR	33.78 ± 4.25	0.817 ± 0.141	0.024 ± 0.017	0.964 ± 0.248
25%	29.58 ± 7.05	0.832 ± 0.114	0.047 ± 0.036	0.901 ± 0.195
25%PET	36.90 ± 4.40	0.893 ± 0.090	0.017 ± 0.012	1.035 ± 0.123
25%PET+MR	37.86 ± 4.16	0.916 ± 0.063	0.015 ± 0.012	1.004 ± 0.126
50%	32.02 ± 8.66	0.865 ± 0.123	0.040 ± 0.036	0.909 ± 0.183
50%PET	39.48 ± 3.90	**0.919 ± 0.067**	0.012 ± 0.008	1.009 ± 0.079
50%PET+MR	**39.88 ± 3.83**	0.896 ± 0.092	**0.012 ± 0.007**	**0.996 ± 0.080**

Figure 3 shows one patient's original 2.5%-, 5%-, 25%-, and 50%-dose PET images and their corresponding synthesized full-dose PET images and prior-synthesized full-dose PET images for the prostate. The average RCNR of the low-dose PET images and MR prior-based synthesized low-dose PET images was close to 1. Moreover, the pelvic contour details of the prior-based synthesized images for doses of 25% and above are visible.

We transferred the synthesized images and MR prior synthesized images for each low-dose image to DICOM format, subtracted each image from the original full-dose PET image matrix, and finally divided the difference matrix by the maximum value of the original image. The resulting image matrixes are shown in Fig. 4. The error between the 25%-dose synthesized images and the prior-synthesized images are within 25%, and the error between the 50%-dose synthesized images and the prior-synthesized images are within 10%.

Six patients were selected from the test set, all of whom had images of prostate or pelvic lesions, as shown in Fig. 5. The figure shows the diffusion weighted (DW) image, apparent diffusion coefficient (ADC) image, T2-weighted image, full-dose image, and various synthesized images. The DW image, ADC image, and T2-weighted image in the MR sequence are important references for clinical diagnosis, and the PET images and MR images are complementary.

In the clinical quantification phase, we selected 32 images with lesions in the pelvis or prostate from the test set for scoring. Table 2 shows the mean and variance of the scored from the two nuclear medicine doctors for PET images of different doses, processed PET images, and prior-based PET images. The average score of the full-dose images MR prior-synthesized from 25%-dose PET images is 0.1 points lower than the average score of the target images. In contrast, the average score of the full-dose images synthesized from 25% dose PET images without the prior is 0.3 points lower than the average score of the target images. In addition, to improve the credibility of the analysis, we combined the scores of the two doctors. When the two nuclear medicine doctors had different scores for the same image, then the lower score of the two was taken. Fig. 6 shows the distribution of this score. When MR images were used as the prior, more than 80% of the full-dose PET images synthesized from 25%-dose PET images had scores of 4, while the rest had scores of 3. When no priors were used, the scores of the full-dose images synthesized from the 25%-dose images indicated that the full-dose images were between good and poor quality. Regardless of whether MR images were used as priors, the scores of the full-dose image synthesized from the 50%-dose PET images were greater than or equal to 4. At each dose, using MR images as priors in synthesizing the images was better than using single low-dose PET images to synthesize full-dose images.

Table 2
Mean clinical quantitative scores from nuclear medicine doctors on low-dose PET images, synthesized full-dose PET images, MR prior-synthesized full-dose PET images, and target images.

	Original	PET	PET+MR
2.5%	1.00 ± 0.00	2.44 ± 0.56	2.69 ± 0.46
5%	1.69 ± 0.46	2.94 ± 0.43	3.28 ± 0.57
25%	2.47 ± 0.50	3.62 ± 0.48	3.84 ± 0.36
50%	3.03 ± 0.39	4.03 ± 0.17	4.03 ± 0.17
100%	3.94 ± 0.24	-	-

Discussion

In the low-dose PET image denoising method, MR images were used as prior image to provide rich tissue and anatomical information for PET image synthesis, thereby improving image quality, contours and details. However, the use of MR as priors can also lead to registration problems. Due to the characteristics of the MR images and the PSMA PET images, accurate registration, regardless of whether rigid registration or flexible registration is used, can be difficult. Data registration is not a problem, however, because the integrated PET/MRI device uses coaxial scanning, and the data it collects can be directly applied to low-dose PET restoration. Theoretically, data collected by integrated PET/MR are more suitable

for MR prior-based low-dose PET estimation than data collected by sequential PET/MR, insert PET/MR, or multiple devices.

When using a single low-dose PET image for denoising, synthesized full-dose prostate images have poor overall contour and edge details and cannot be restored well. When including MR images as priors for low-dose PET image denoising, the edges of PET images with a dose of less than 5% is blurred, and the surrounding contours are not clear, which can affect the diagnosis. In PET images with a dose higher than 5%, the shape and edges of the key parts of the prostate are clear, the contours of the surrounding organs are distinct, the contrast is relatively close to that of the target image, and the clinical quantitative score is the same as that of the target image. The 25%- and 50%-dose PET images synthesized based on the MR priors showed sufficient quality to meet the requirements for clinical analysis.

However, our method still has certain limitations. First, the proposed network uses the Haar wavelet transform for up- and downsampling. Other potential wavelet transforms include Gaussian, Morlet, Shanno, and other transformation methods, and whether the Haar wavelet transform is the most suitable for MR prior-based low-dose PET estimation is not yet known. Second, the proposed network has a significant effect on low-dose PET images with good overall characteristics but has a poor effect on low-dose PET images with inconspicuous overall characteristics. The recovery effect of the convolutional neural network on PET images with a dose of 5% and below needs to be improved; for example, the use of generative adversarial neural networks for image recovery and PET/MR examinations could reduce the dose even further.

Conclusion

In conclusion, we used a convolutional neural network combining discrete wavelet transform and convolution methods to estimate full-dose PET images from PSMA low-dose image collected by PET/MR. After clinical quantitative analysis and objective image index analysis, the deep learning method we proposed was shown to be capable of synthesizing a full-dose image from 25%-dose PSMA PET images collected by PET/MR, indicating that the dose can be reduced by 75%.

Declarations

Funding This work was supported by the National Natural Science Foundation of China (32022042, 81871441), the Shenzhen Excellent Technological Innovation Talent Training Project of China (RCJC20200714114436080), and the Natural Science Foundation of Guangdong Province in China (2020A1515010733).

Compliance with ethical standards

Ethics approval: All procedures performed in studies involving human participants were in accordance with the ethical standards of the Nanjing First Hospital research committee and with the 1964 Helsinki declaration and its later amendments or comparable ethical standards.

Conflict of interest: Hongwei Sun, Jianmin Yuan, and Qiang He are employees of the United Imaging Healthcare group. The other authors have no conflict of interest.

Informed consent: The requirement for informed consent was waived.

References

1. Sung H, Ferlay J, Siegel RL, et al. Global Cancer Statistics 2020: GLOBOCAN Estimates of Incidence and Mortality Worldwide for 36 Cancers in 185 Countries. *CA: A Cancer Journal for Clinicians.* 2021; 71: 209-249.
2. Eiber M, Weirich G, Holzapfel K, et al. Simultaneous 68Ga-PSMA HBED-CC PET/MRI Improves the Localization of Primary Prostate Cancer. European Urology. 2016;70:829–36.
3. Hicks RM, Simko JP, Westphalen AC, et al. Diagnostic Accuracy of 68Ga-PSMA-11 PET/MRI Compared with Multiparametric MRI in the Detection of Prostate Cancer. Radiology. 2018;289:730–7.
4. Park SY, Zacharias C, Harrison C, et al. Gallium 68 PSMA-11 PET/MR Imaging in Patients with Intermediate- or High-Risk Prostate Cancer. Radiology. 2018;288:495–505.
5. Murthy V, Sonni I, Jariwala N, et al. The Role of PSMA PET/CT and PET/MRI in the Initial Staging of Prostate Cancer. European Urology Focus. 2021;7:258–66.
6. Grubmüller B, Baltzer P, Hartenbach S, et al. PSMA Ligand PET/MRI for Primary Prostate Cancer: Staging Performance and Clinical Impact. Clinical Cancer Research. 2018;24:6300.
7. Kranzbühler B, Nagel H, Becker AS, et al. Clinical performance of 68Ga-PSMA-11 PET/MRI for the detection of recurrent prostate cancer following radical prostatectomy. European Journal of Nuclear Medicine Molecular Imaging. 2018;45:20–30.
8. Wang R, Shen G, Yang R, Ma X, Tian R. 68Ga-PSMA PET/MRI for the diagnosis of primary and biochemically recurrent prostate cancer: A meta-analysis. European Journal of Radiology. 2020;130:109131.
9. Vandenberghe S, Marsden PK. PET-MRI: a review of challenges and solutions in the development of integrated multimodality imaging. Physics in Medicine Biology. 2015;60:R115.
10. An L, Zhang P, Adeli E, et al. Multi-level canonical correlation analysis for standard-dose PET image estimation. IEEE Transactions on Image Processing. 2016;25:3303–15.
11. Wang Y, Zhang P, An L, et al. Predicting standard-dose PET image from low-dose PET and multimodal MR images using mapping-based sparse representation. Physics in Medicine Biology. 2016;61:791–812.
12. Xiang L, Qiao Y, Nie D, et al. Deep auto-context convolutional neural networks for standard-dose PET image estimation from low-dose PET/MRI. Neurocomputing. 2017;267:406–16.
13. Wang Y, Yu B, Wang L, et al. 3D conditional generative adversarial networks for high-quality PET image estimation at low dose. NeuroImage. 2018;174:550–62.

14. Cui J, Gong K, Guo N, et al. PET image denoising using unsupervised deep learning. European Journal of Nuclear Medicine Molecular Imaging. 2019;46:2780–9.
15. Yang L, Xue D, Tonghe W, et al. "Estimating standard-dose PET from low-dose PET with deep learning," in *Proc.SPIE*, 2020, 11313.
16. Zhou L, Schaefferkoetter JD, Tham IWK, Huang G, Yan J. Supervised learning with cyclegan for low-dose FDG PET image denoising. Medical Image Analysis. 2020;65:101770.
17. Liu W, Yan Q, Zhao Y "Densely self-guided wavelet network for image denoising," in *Proceedings of the IEEE/CVF Conference on Computer Vision and Pattern Recognition Workshops*, 2020 432-433.
18. Gregory R. Lee RG, Wasilewski F, Wohlfahrt K. Aaron O'Leary. PyWavelets: A Python package for wavelet analysis. Journal of Open Source Software. 2019;4:1237.
19. Park B, Yu S, Jeong J "Densely connected hierarchical network for image denoising," in *Proceedings of the IEEE/CVF Conference on Computer Vision and Pattern Recognition Workshops*, 2019 0-0.
20. Ouyang J, Chen KT, Gong E, Pauly J, Zaharchuk G. Ultra-low-dose PET reconstruction using generative adversarial network with feature matching and task-specific perceptual loss. Medical Physics. 2019;46:3555–64.
21. Chen KT, Gong E, de Carvalho Macruz FB, et al. Ultra–Low-Dose 18F-Florbetaben Amyloid PET Imaging Using Deep Learning with Multi-Contrast MRI Inputs. Radiology. 2018;290:649–56.

Figures

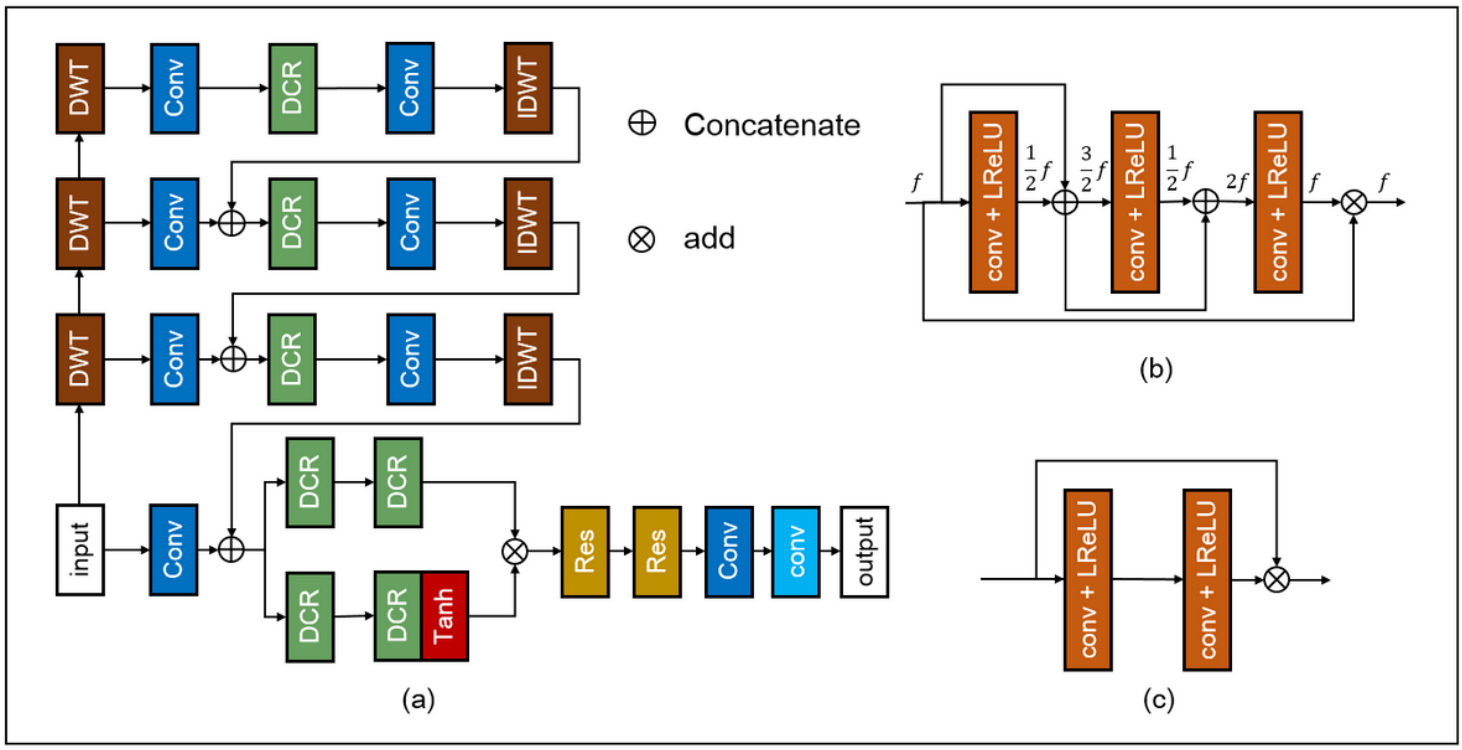

Figure 1

Discrete-wavelet-transform neural network (DWTN), including (a) the structure of the DWTN network, (b) the structure of the densely connected residual (DCR) block, and (c) the structure of the residual block

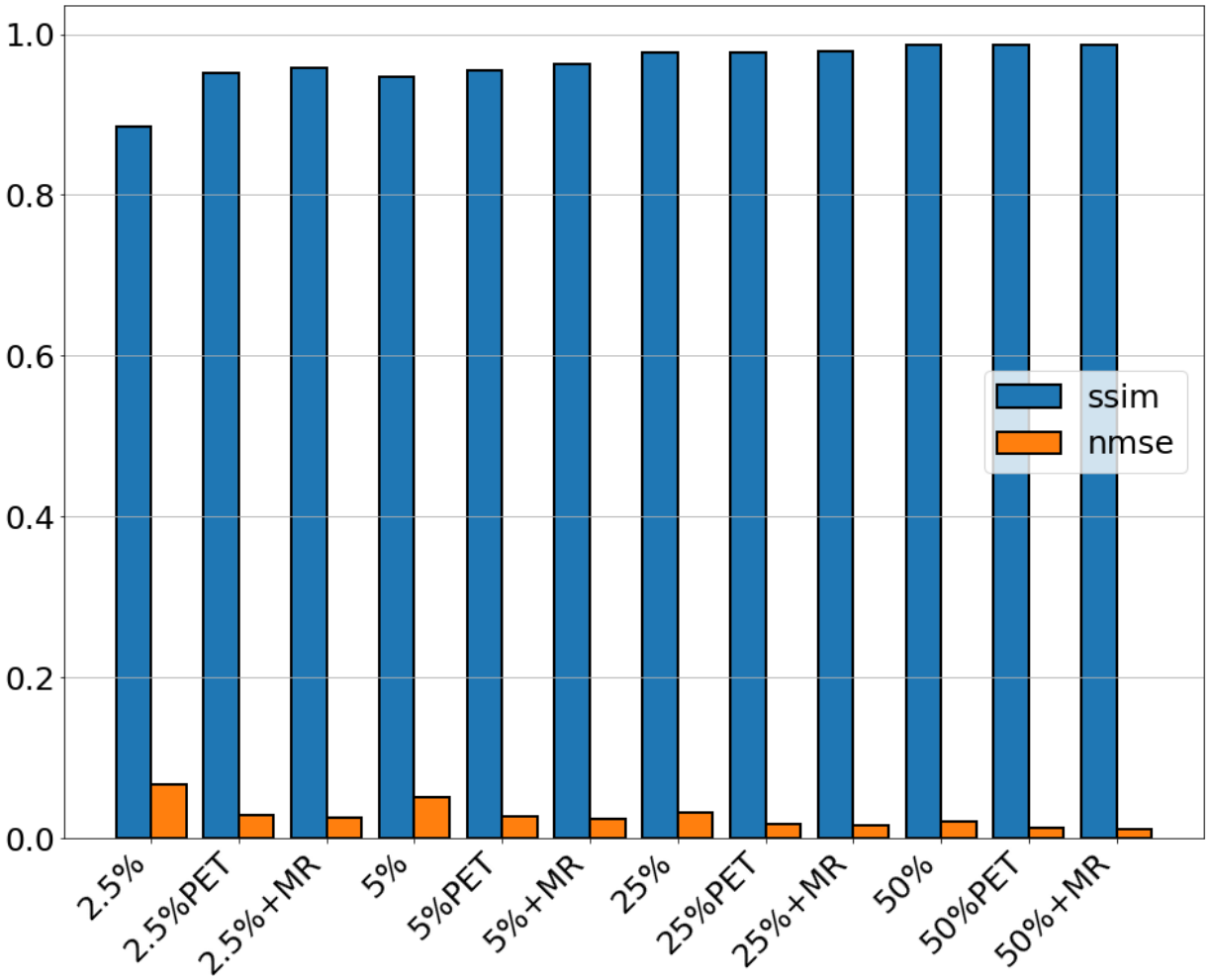

Figure 2

NMSE and SSIM of the original low-dose PET images, synthetic full-dose PET images, and MR prior-synthesized full-dose PET images at all doses, where blue represents SSIM, orange represents NMSE, and different degrees of color represent images of different doses

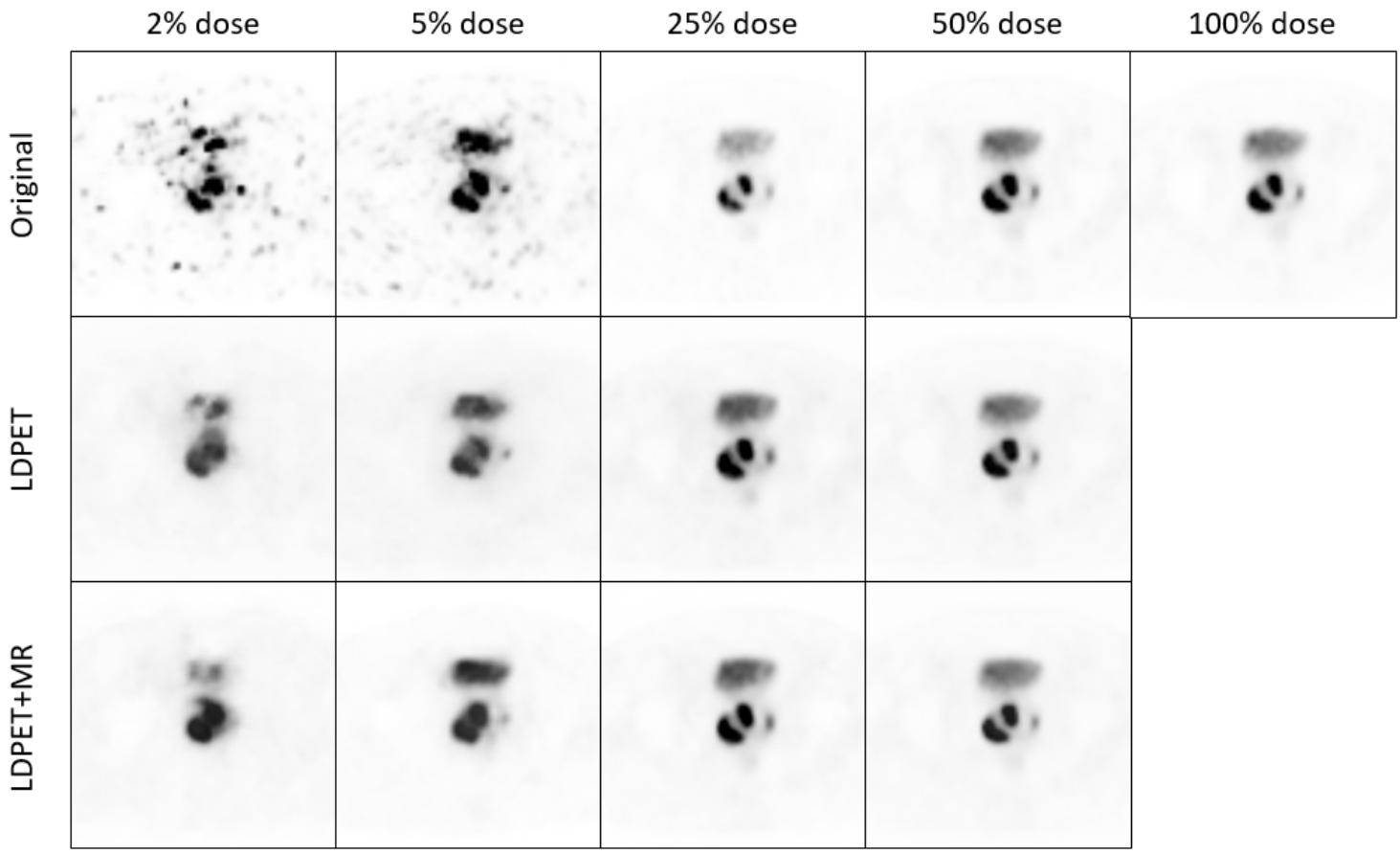

Figure 3

The original low-dose PET images, synthesized full-dose PET images, MR prior-synthesized full-dose PET images of all doses, and their ROIs

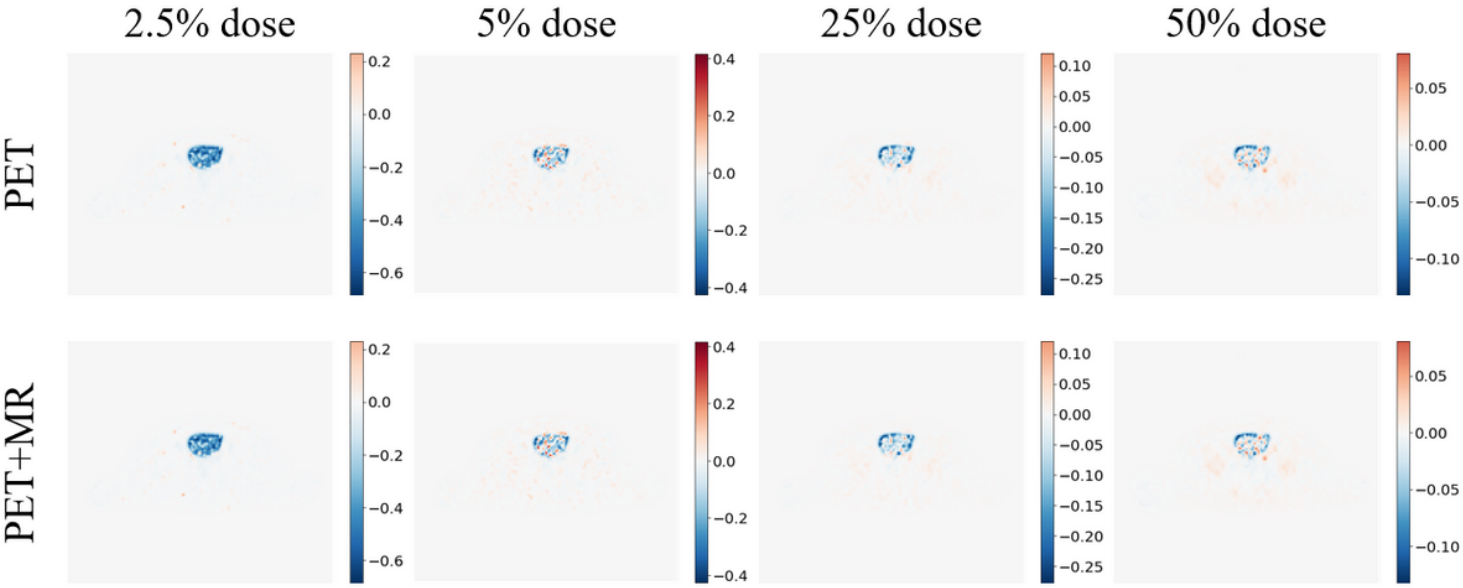

Figure 4

Synthesized full-dose PET image, MR prior for all doses, combined full-dose PET image and target subtraction difference map and original image

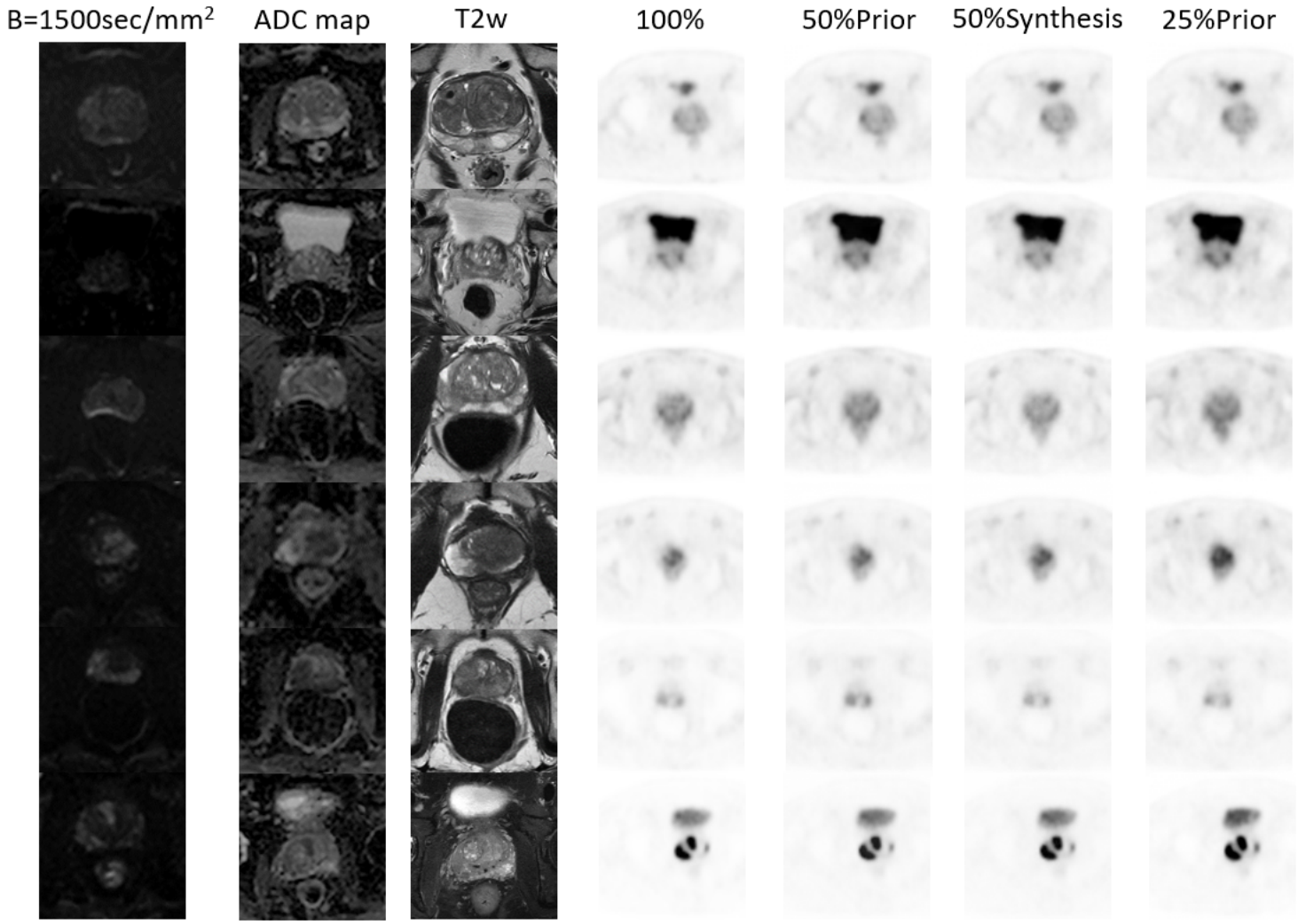

Figure 5

MR and PET images of 6 patients with prostate or pelvic lesions from the test set. The MR sequences included DW-, ADC- and T2-weighted images. The PET images consist of the original full-dose images, full-dose images synthesized from 50%-dose images with MR priors, full-dose images synthesized from 50%-dose images without MR priors, and full-dose images synthesized from 25%-dose images with MR priors.

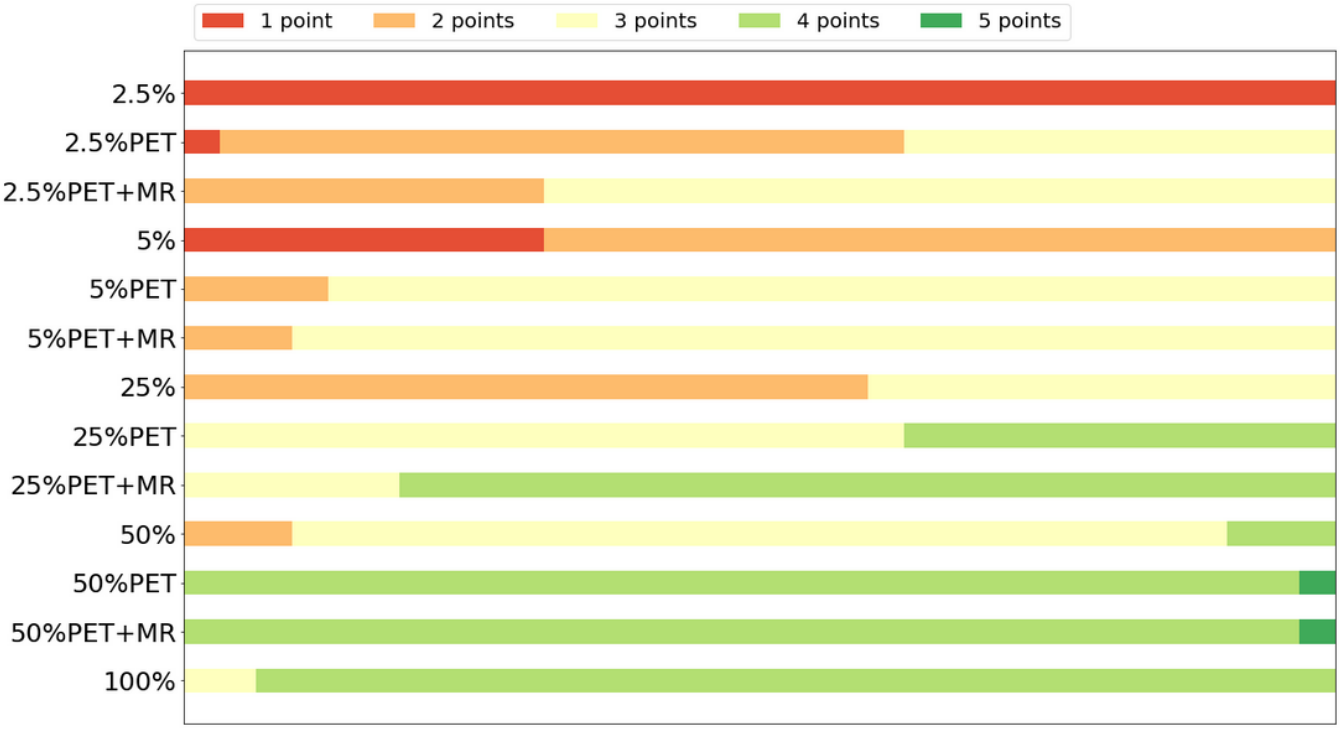

Figure 6

Distribution of clinical quantitative scores from nuclear medicine doctors on low-dose PET images, synthesized full-dose PET images, MR prior-synthesized full-dose PET images, and target images.